Carbohydrate Polymers 110 (2014) 238–252

Contents lists available at ScienceDirect

Carbohydrate Polymers

journal homepage: www.elsevier.com/locate/carbpol

Porous silicon-cyclodextrin based polymer composites for drug delivery applications

J. Hernandez-Montelongo[a,*], N. Naveas[a,1], S. Degoutin[b,2], N. Tabary[b,2], F. Chai[c,3], V. Spampinato[d,4], G. Ceccone[d,4], F. Rossi[d,4], V. Torres-Costa[a,1], M. Manso-Silvan[a,1], B. Martel[b,2]

[a] Departamento de Física Aplicada, Universidad Autónoma de Madrid, 28049, Madrid, Spain
[b] Unité Matériaux Et Transformations (UMET), Ingénierie des Systèmes Polymères, Université Lille 1, F-59655, Villeneuve D'Ascq, France
[c] Groupe de Recherche sur Biomatériaux (U 1008 INSERM) Faculté de Médecine, Université Lille 2, F-59045, Lille, France
[d] European Commission, Joint Research Centre, Institute for Health and Consumer Protection, 21020, Ispra (Va), Italy

ARTICLE INFO

Article history:
Received 26 November 2013
Received in revised form 19 March 2014
Accepted 2 April 2014
Available online 13 April 2014

Keywords:
Porous silicon
β-Cyclodextrin–citric acid polymer
Composites
Drug delivery

ABSTRACT

One of the main applications of porous silicon (PSi) in biomedicine is drug release, either as a single material or as a part of a composite. PSi composites are attractive candidates for drug delivery systems because they can display new chemical and physical characteristics, which are not exhibited by the individual constituents alone. Since cyclodextrin-based polymers have been proven efficient materials for drug delivery, in this work β-cyclodextrin–citric acid *in-situ* polymerization was used to functionalize two kinds of PSi (nanoporous and macroporous). The synthesized composites were characterized by microscopy techniques (SEM and AFM), physicochemical methods (ATR-FTIR, XPS, water contact angle, TGA and TBO titration) and a preliminary biological assay was performed. Both systems were tested as drug delivery platforms with two different model drugs, namely, ciprofloxacin (an antibiotic) and prednisolone (an anti-inflammatory), in two different media: pure water and PBS solution. Results show that both kinds of PSi/β-cyclodextrin–citric acid polymer composites, nano- and macro-, provide enhanced release control for drug delivery applications than non-functionalized PSi samples.

1. Introduction

Porous silicon (PSi) is an excellent biomaterial due to its high surface area (Bisi, Ossicini, & Pavesi, 2000), biocompatibility (Martin-Palma, Manso-Silvan, & Torres-Costa, 2010), biodegradability (Tanaka et al., 2010) and bioresorbability (Hernández-Montelongo, Muñoz-Noval, Torres-Costa, Martín-Palma, & Manso-Silvan, 2012). In view of these properties, different PSi bioapplications have been developed such as: biosensing (Dhanekar & Jain, 2013a), tissue engineering (Coffer et al., 2005), tumor imaging (Martin-Palma et al., 2010), bioreactor platform (Stewart & Buriak, 2000) and drug delivery (Anglin, Cheng, Freeman, & Sailor, 2008). When PSi is used as a drug delivery system, drugs are loaded into its porous matrix or immobilized on its surface after a proper surface derivatization (Stewart & Buriak, 2000). However, when combined with biopolymers, it works as substrate for composite materials, providing new advantageous chemical and physical characteristics, which are not exhibited by the individual constituents, such as an improved control over drug release kinetics and improved stability in aqueous solution (Anglin et al., 2008). Indeed, PSi has been previously combined with biopolymers such as polylactide, polydimethylsiloxane, polyethylene, polystyrene, polycaprolactone and poly(N-isopropylacrylamide) for that purpose (Anglin et al., 2008; Mukherjee et al., 2006; Segal et al., 2007).

Herein, we focus on the functionalization of PSi by β-cyclodextrin (βCD). Cyclodextrins (CDs) are cyclic oligosaccharides with a hydrophilic outer surface (C–OH groups) and a hydrophilic apolar cavity (C–O–C and C–H bonds) (Davis & Brewster, 2004) (Fig. 1). Because of their characteristic cavity and their ability to form reversible complexes with drugs, CDs have been used as efficient delivery carriers (Leprêtre et al., 2009). CDs have also been crosslinked, yielding a three-dimensional polymer network suitable for drug delivery applications. Such volume structure presents

* Corresponding author. Tel.: +34 91497 8608; fax: +34 91 497 3969.
E-mail address: jacobo.hernandez@uam.es (J. Hernandez-Montelongo).
[1] Tel.: +34 91497 8608; fax: +34 91 497 3969.
[2] Tel.: +33 0 320 43 49 67; fax: + 33 0 320 43 65 91.
[3] Tel.: +33 0 320 96 49 75; fax: +33 0 320 96 49 95.
[4] Tel.: +39 0332 78 9338; fax: +39 0332 78 5730.

http://dx.doi.org/10.1016/j.carbpol.2014.04.002
0144-8617/

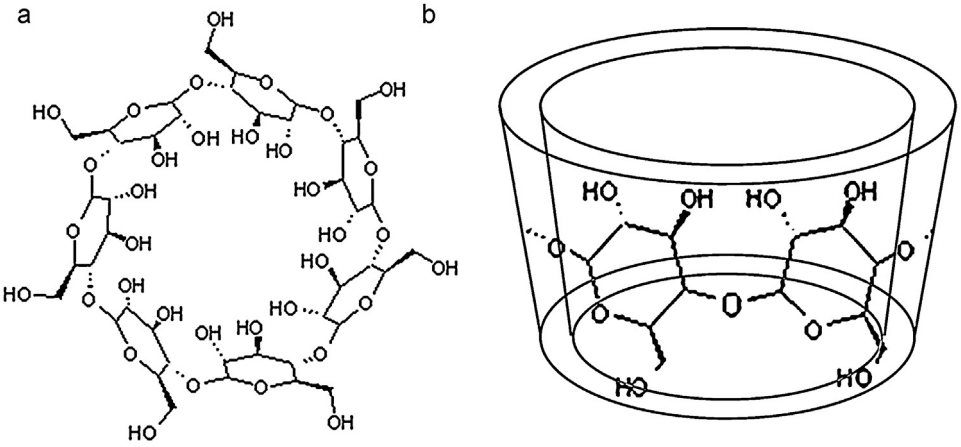

Fig. 1. (a) Chemical structure of β-CD, and (b) its toroidal shape.

extended interactions with drugs, prolonging residence time in the medium and/or increasing efficiency and specificity towards targeted sites (Trotta, Zanetti, & Cavalli, 2012). Some examples used crosslinkers used to polymerize CDs are alginate (Izawa et al., 2013), poly(ethylene oxide) (Liu et al., 2011; Li, Ni, & Leong, 2003), camptothecin (Davis, 2009), epichlorohydrin (Davis & Brewster, 2004), and citric acid (Martin et al., 2013), which is the one used here, amongst others. In addition, CD-based polymers have been used to functionalize different biomaterials for drug release applications, such as vascular prostheses (Blanchemain et al., 2012), polypropylene (Degoutin et al., 2012), polyamide inguinal plates (El Ghoul et al., 2008), hydroxyapatite (Leprêtre et al., 2009) and hip prostheses (Taha et al., 2013).

All these features make CDs interesting for combining with PSi for further drug delivery applications. In this work, the functionalization of nanoporous and macroporous PSi (nPSi and mPSi, respectively) by β-CD–citric acid (CTR) *in-situ* polymerization has been investigated. In order to test their viability as drug delivery systems (Thrimawithana, Young, Bunt, Green, & Alany, 2011), these composites have been loaded with two model drugs: ciprofloxacin (CFX, an antibiotic) (Oliver, Strube, Mohan, & Slomovic, 2005; Ravindran et al., 2009) and prednisolone (PDN, an anti-inflammatory) (Lane & Holland, 2012; Struck & Bariszlovich, 2001), in two media: pure water and PBS solution.

2. Materials and methods

2.1. Porous silicon preparation

2.1.1. Nanoporous silicon

Nanoporous silicon (nPSi) was fabricated by electrochemical etching of p^+ type silicon wafers (boron-doped, orientation ⟨1 0 0⟩, resistivity 0.01–0.02 Ω cm) in a HF:EtOH (1:2) solution, HF at 48 wt%. A current density of 60 mA cm^{-2} was applied for 90 s under illumination with a 150 W halogen lamp (Hernández-Montelongo et al., 2012). Afterwards, nPSi was chemically oxidized (nPSi-CO_x) by H_2O_2 (30%, v/v) for 2 h (Naveas et al., 2012), rinsed with EtOH and dried with a nitrogen flow. A porosity of 60% for these samples was calculated by gravimetric analysis.

2.1.2. Macroporous silicon

Macroporous silicon (mPSi) was fabricated by electrochemical etching of p^+ type silicon wafers (boron-doped, orientation ⟨1 0 0⟩, resistivity 29–31 Ω cm) in a HF:DMF (1:6) solution, HF at 48 wt% (Föll, Christophersen, Carstensen, & Hasse, 2002). In this case, the applied current density was 20 mA cm^{-2} for 600 s under illumination with the same 150 W halogen lamp. The mPSi samples were also chemically oxidized (mPSi-CO_x) by H_2O_2 (30%, v/v) for 2 h, rinsed with EtOH and dried with nitrogen. In these samples a 40% porosity was determined by gravimetric analysis.

As-prepared (fresh) PSi surface is mainly composed of Si–H bonds (Bisi et al., 2000; Mawhinney, Glass, & Yates, 1997; Tolstoy, Chernyshova, & Skryshevsky, 2003). The chemical post-treatment of PSi by H_2O_2 is an oxidation process involving different reactions; Si–H bonds can be transformed to Si–OH, Si–O–Si or $-O_ySi-H_x$. The oxidation process is represented by Eq. (1) (Dhanekar & Jain, 2013b; Naveas et al., 2012):

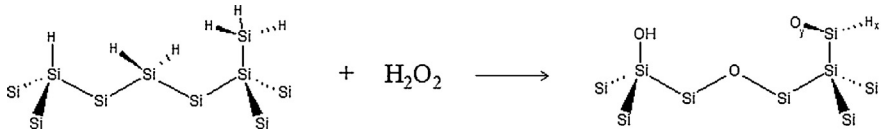

(1)

2.2. PSi functionalization with modified β-cyclodextrin

The proposed method to functionalize both kinds of PSi is straight forward and accessible (Fig. 2). A monomer solution was prepared with 10 g β-cyclodextrin (Roquette, Lestrem France), 3 g $NaH_2PO_2{\cdot}H_2O$ (Aldrich, Saint Quentin Fallavier, France) as catalyst and 10 g citric acid (Aldrich, Saint Quentin Fallavier, France) in 100 mL of distilled water. nPSi-CO_x and mPSi-CO_x samples were immersed in this solution for 15 min while stirring. Afterwards, the excess of monomer solution was carefully removed by capillarity using a soft cellulosic tissue, leaving a thin film on the top. The samples were dried, first at room temperature, and later at 90 °C for 1 h in each case. The βCD–CTR polymerization (Martel, Ruffin, Weltrowski, Lekchiri, & Morcellet, 2005) in PSi samples was carried out at 140 °C for 25 min, thereby obtaining the nPSi-CD and mPSi-CD samples. Afterwards, they were washed with distilled water for 15 min while stirring, rinsed with EtOH and dried at 90 °C for 1 h.

The polymerization achieved between βCD and CTR may be explained by a polyesterification mechanism between hydroxyl groups of βCD and carboxylic groups of CTR, which contains three carboxylic groups as detailed in the following equation (Eq. (2)) (Martel et al., 2005). The resulting polymer was named polyCTR–βCD.

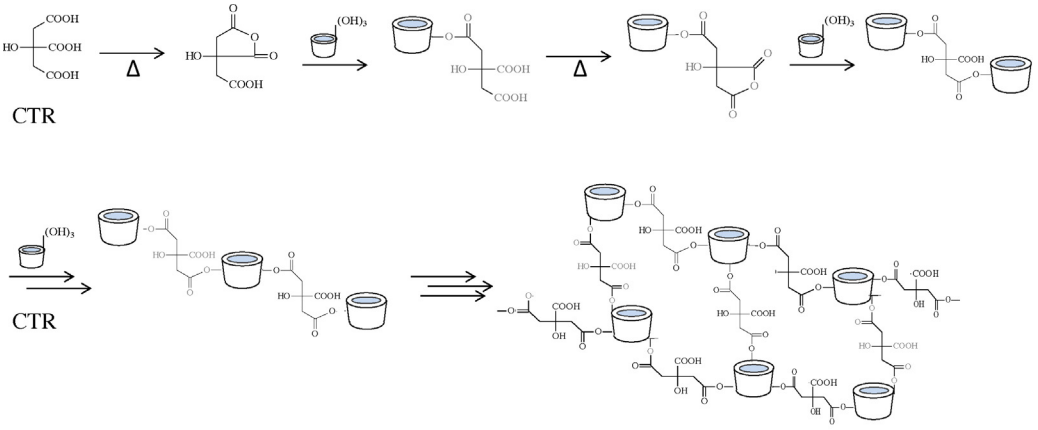

(2)

2.3. Microscopic characterization

The morphology of PSi and polymer layers were studied by using a field-emission scanning electron microscope (FESEM; Philips XL-40FEG) and a conventional scanning electron microscope (SEM; Hitachi S-3000N), operated at 10 keV and 20 keV, respectively.

The roughness and topography of the PSi layers, before and after functionalization with polyCTR–βCD, were assessed by atomic force microscopy (AFM) in tapping mode. A NT-MDT Solver equipped with a Smena head and Si cantilevers (force constant 5 N/m, first harmonic frequency of 158 kHz) was used. To generate topographical images and to calculate sample roughness, the NT-MDT SPM Software was used on scanning areas of 4 μm × 4 μm.

2.4. Physicochemical techniques

Attenuated Total Reflectance Fourier-Transform Infra Red Spectroscopy (ATR-FTIR) was used for PSi surface characterization after its modification. An FTIR spectrometer (Spectrum One, Lita detector, MIR source) was used in the range between 4000 and 650 cm^{-1} with a resolution of 1 cm^{-1} (NS = 4).

In order to obtain a more detailed chemical composition of the samples, X-ray photoelectron spectroscopy (XPS) characterization was carried out. Measurements were performed with an AXIS ULTRA Spectrometer (KRATOS Analytical, UK). The samples were irradiated with monochromatic AlKα X-rays ($h\nu$ = 1486.6 eV). The area of analysis was 400 μm × 700 μm and the take-off angle (TOA) was fixed at 90° with respect to the sample surface. Pass energies of 160 eV and 20 eV were used for the survey and core level spectra,

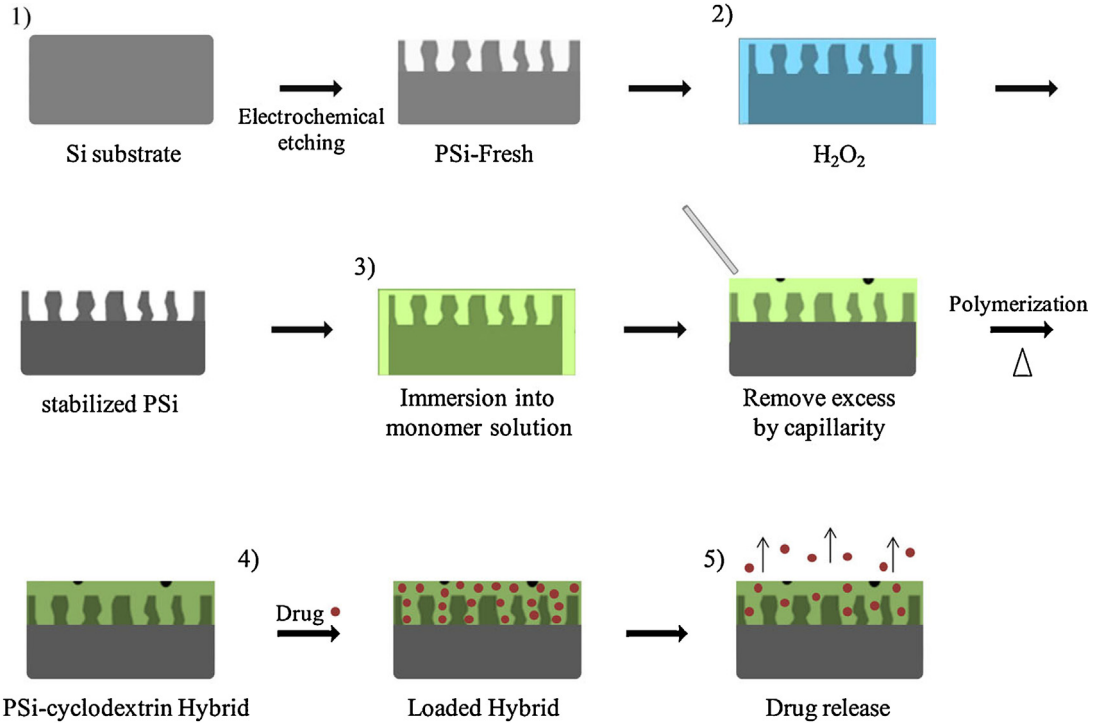

Fig. 2. Fabrication scheme of porous silicon-cyclodextrin composite drug delivery systems: (1) synthesis of nano and micro porous structures, (2) chemical oxidization, (3) cyclodextrin polymerization, (4) drug loading, and (5) drug release.

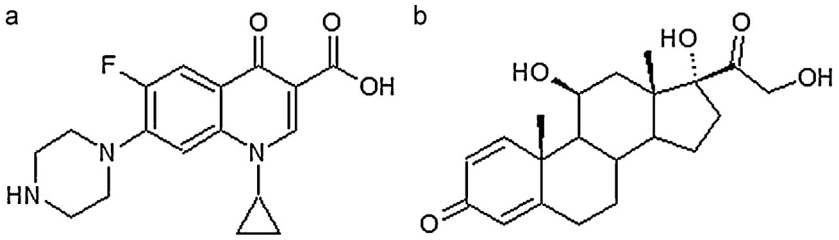

Fig. 3. Scheme of: (a) CFX, ciprofloxacin; and (b) PDN, prednisolone.

respectively. A filament (I = 1.9 A, V = 3.2 V) inserted in the magnetic lens system acts as neutralizer for surface charge compensation. All core level spectra were shifted to a common binding energy of the hydrocarbon component of the C1s spectra of 285.0 eV. The data were processed using the Vision2 software (Kratos, UK) and CasaXPS v3.15 (Casa Software, UK).

In order to evaluate the surface wettability of the samples, a water contact angle measuring system (KSV CAM-101) was used on the static sessile drop mode. Statistical data were processed by Statgraphics Centurion XV.

The thermogravimetric analyses (TGA) were performed on a TA-Q50 system (TA Instruments) to determinate the quantity of organic polyCTR–βCD fixed onto the PSi samples. Measurements were recorded in the 30–700 °C temperature range with a heating rate of 10 °C/min in a 90% O_2–10% N_2 atmosphere.

As polyCTR–βCD presents free carboxylate groups carried by the citrate crosslinks, the carboxylic group density on the PSi surface (μmol COOH/cm^2 and μmol COOH/mg) was calculated using toluidine blue ortho (TBO) titration, (Degoutin et al., 2012) which was detected by using a UV-1800 spectrometer (Shimadzu) at 634 nm. The density of COOH groups on modified PSi supports was calculated according to a mole-to-mole complex between TBO and accessible COOH groups.

2.5. Cytocompatibility

As a first preliminary study of the cytocompatibility of the composites, the human epithelial cell (L132) culture was selected. First, cells were cultured in Eagle's minimum essential medium (MEM, ATCC®) with glutamax (Gibco BRL) supplemented with 10% fetal calf serum (FCS, Gibco); 50 μg/ml gentamicin (Gibco) and 1 μg/ml amphotericin B (Gibco). Later, cells were incubated at 37 °C and 5% CO_2 atmosphere and 100% relative humidity. The cells in the phase of exponential growth were seeded on the samples and cultured for 24 h. For the observation of cell adhesion and cell morphology with scanning electron microscopy (SEM), the samples were fixed with 2.5% glutaraldehyde in 0.1 M sodium phosphate buffer (pH 7), then washed twice in 0.1 M sodium phosphate buffer. Thereafter, the samples were post-fixed with 1% osmium tetroxide (OsO_4) in saturated $HgCl_2$ to obtain the best cell morphology. After a graduated dehydration in ethanol, the samples were critical-point dried with CO_2 and examined in a J-SM-5300 SEM (Jeol), operated at 30 keV.

2.6. Drug release profiles

Samples were loaded with ciprofloxacin-base (CFX, an antibiotic) and prednisolone (PDN, an anti-inflammatory) (both in Fig. 3), by means of a saturated aqueous solution of each drug (60 mg/l and 200 mg/l, respectively) for 24 h stirring at 100 rpm. CFX was obtained from Bayer Health Care (Leverkusen, Germany) and PDN was purchased from Sigma-Aldrich (Saint Quentin Fallavier, France). Drug loaded samples were placed into vials filled with 5 mL of distilled water or PBS in a horizontal shaker (100 rpm) (Innova® 40, New Brunswick Scientific, Le Pecq, France). At pre-determined time intervals, the supernatant solution was completely renewed and the drug content in the withdrawn bulk fluid determined by UV-spectrophotometry (UV-1800 Shimadzu) (Leprêtre et al., 2009): CFX was detected at 275 nm and the PDN at 245 nm. All experiments were conducted in triplicate and non loaded samples were used as controls in these kinetic experiments.

In order to determine the mechanism of drug release, the Korsmeyer–Peppas semi-empirical model (Korsmeyer, Gurny, Doelker, Buri, & Peppas, 1983) was fitted to the release profiles:

$$\frac{M_t}{M_\infty} = kt^n \quad (3)$$

where M_t/M_∞ is the fractional drug release, t is the release time, k is a kinetic constant characteristic of the drug/polymer system and

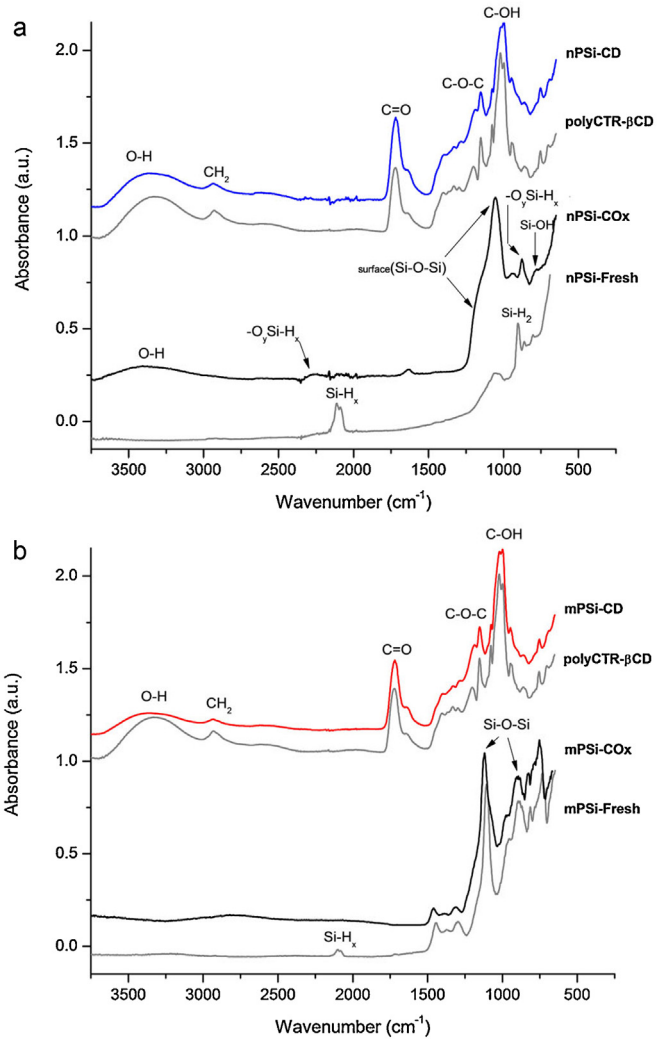

Fig. 4. FTIR-ATR spectra of: (a) nPSi-series samples and (b) mPSi-series samples.

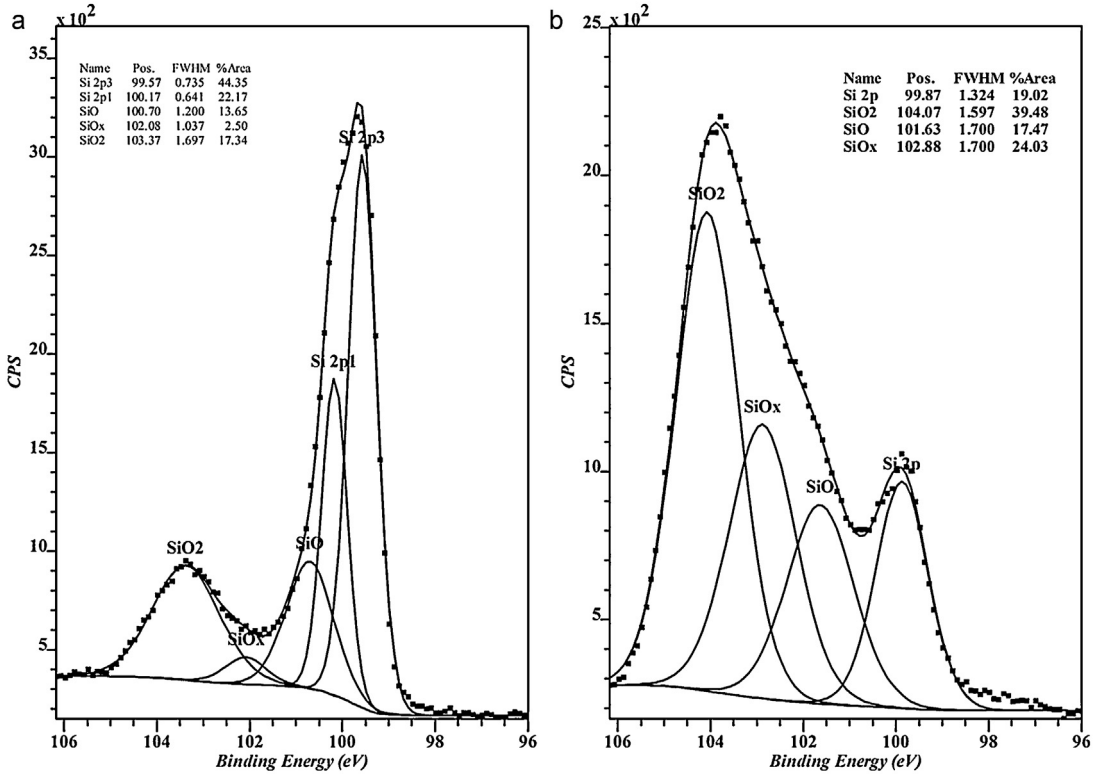

Fig. 5. S2p core level XPS spectra of: (a) nPSi and (b) nPSi-CO_x.

n is an exponent which characterizes the mechanism of release. Eq. (3) is useful for a generalized analysis of release data, although it may only be used up to 60% of the drug released (Lucht & Peppas, 1987). The fitting model was conducted with OriginPro 8 software.

3. Results and discussion

3.1. Functionalization of PSi by polyCTR–βCD

In order to determine the chemical composition of the samples, ATR-FTIR analyses were carried out as shown in Fig. 4. Spectra plotted in Fig. 4a correspond to nano-series. The spectrum corresponding to nPSi presents absorption bands at 2141, 2115, and 2090 cm^{-1}, which are attributed to Si–H_x (x = 1, 2, 3) stretching modes, respectively (Mawhinney et al., 1997). The band assignment to SiH_2 scissor mode was also detected at 906 cm^{-1} (Tolstoy et al., 2003). As it was mentioned in Section 2.1, Si–H bonds are a characteristic of fresh PSi. After the chemical treatment (nPSi-CO_x), the bands corresponding to Si–H bonds changed into bands assigned to surface –O_ySi–H_x, due to the oxidation process: at 2250 cm^{-1} for stretching mode and at 880 cm^{-1} for bending mode (Tolstoy et al., 2003; Mawhinney et al., 1997). Also, a weak band at 835–795 cm^{-1} from the Si–OH bond can be observed (Naveas et al., 2012) as well as the O–H stretching band from SiOH groups at 3350 cm^{-1} (Tolstoy et al., 2003). The bands related to surface Si–O–Si stretching mode at 1170 and 1060 cm^{-1} were also observed (Tolstoy et al., 2003; Mawhinney et al., 1997). These results are in agreement with Eq. (1) of Section 2.1.

Nanoporous samples functionalized with polyCTR–βCD (nPSi-CD) exhibit the same bands as pure polyCTR–βCD. The main band corresponding to bond vibrations from βCD–CTR polymer (Martin et al., 2013; Zhao, Zhao, Zhu, Tian, & Shen, 2009) can be observed: O–H stretching from hydroxyl and carboxyl groups (3435 cm^{-1}), CH_2 asymmetric stretching (2933 cm^{-1}), C=O stretching (1736 cm^{-1}), C–O–C stretching (1155 cm^{-1}) and the C–OH stretching (1026 cm^{-1}). This indicates that the nanostructured PSi was properly functionalized.

FTIR spectra of macroporous samples are plotted in Fig. 4b. In the mPSi spectrum a weak band at 2100 cm^{-1} is appreciable. This band is also related to Si–H bonds from fresh PSi (Gorbanyuk, Evtukh, Litovchenko, Solnsev, & Pakhlov, 2006). In this case, the band can be decomposed into three bands near 2140, 2110 and 2080 cm^{-1} (Gorbanyuk et al., 2006). Nevertheless, the main absorption peaks correspond to Si–O–Si at 1108 cm^{-1} and 870 cm^{-1} (Mawhinney et al., 1997; Ogata, Niki, Sakka, & Iwasaki, 1995), confirming that mPSi is more susceptible to oxidation than to hydrogenation during its formation (Föll et al., 2002; Gorbanyuk et al., 2006). After chemical oxidation, the Si-H signal faded away and SiOH groups were not detected. As in the case of nPSi-CD, mPSi-CD samples were properly functionalized, as shown by the fact that their spectra match that of pure βCD–CTR polymer.

Since XPS probing depth in our experimental conditions was approximately 10–12 nm, the study of the evolution of the surface chemistry was performed on the nPSi series samples (the root mean square roughness 1–10 nm being below the analysis depth). The elemental surface composition of the nPSi, nPSi-CO_x and nPSi-CD was obtained from the XPS survey spectra and are presented in Table 1.

It can be seen that the starting nPSi substrate shows C contamination, part from the expected Si and O signals. Moreover, a light presence of other surface synthesis residues, such as F, were also detected. After oxidation, C and Si content drastically reduced, but the O content increased by a factor of 2.1. This indicates the successful oxidation of the PSi surface. This result was also confirmed by the analysis of the Si 2p core level spectra (Fig. 5a), where it can be noticed that the doublet at about 99.6 eV ($Si2p_{3/2}$), corresponding to the Si^0 oxidation state strongly decreases. In parallel, the other components at higher binding energies,

Table 1
Surface chemical compositions of nPSi, nPSi-CO_x and nPSi-CD obtained from XPS analysis.

Sample	C (at%)	O (at%)	N (at%)	Si (at%)	F (at%)
nPSi	22.5 (±0.2)	31.6 (±0.03)	–	44.9 (±0.41)	1.0 (±0.2)
nPSi-CO_x	2.5 (±0.4)	66.2 (±0.24)	–	30.7 (±0.5)	0.6 (±0.1)
nPSi-CD	56.9 (±0.5)	43.0 (±0.24)	–	–	–

corresponding to different oxidation states increased. In particular, for the bare nPSi, three components related to SiO (100.7 eV), SiO_x ($x < 2$, 102 eV) and SiO_2 (103.6 eV) were obtained by curve fitting (Seah et al., 2004). After the oxidation, the major component of nPSi-CO_x is related to SiO_2 groups, which accounts for about 40% of the Si signal (Fig. 5b). Moreover, the position of the SiO_2 peak shifts towards higher binding energies (0.6 eV respect to the bare nPSi), indicating the growth of a dense oxide layer (Ulgut & Suzer, 2003). However, it should be noticed that signal intensities of components corresponding to lower Si oxidation states and to sub-stoichiometric SiO_x bonds also increased after the oxidation process.

The *in-situ* polymerization of βCD and CTR further changes the surface composition (Table 1). In fact, the Si signal disappeared, the O signal decreased and became the dominant element, indicating the successful growth of a uniform and continuous polymer layer. This result is also corroborated by the C1s core level spectrum presented in Fig. 6. The C1s envelope can be fitted with four components corresponding to C–C/CH (285.00 eV), C–O (286.5 eV), C=O/O–C–O (287.5 eV) and COOH/R (289.2 eV) (Bemason, 1992; Ulgut & Suzer, 2003). The successful surface polymerization was possible due to the previous oxidation process, which stabilizes the PSi and makes the interaction with the polymerized CDs possible.

The samples surface wettability was assessed by water contact angle measurements (Fig. 7). As expected, nPSi and mPSi samples showed a hydrophobic behavior (126° and 84°, respectively) due to Si–H surface groups (Low, Williams, Canham, & Voelcker, 2006). After chemical oxidation, fresh samples changed their wettability into a strong hydrophilic behavior, 7.7° for nPSi-CO_x and 14.7° for mPSi-CO_x, due to Si–O, H–Si–O (Low et al., 2006) and Si–OH bonds (Noval et al., 2012). In the case of functionalized samples, the wettability was practically the same on both (31° for nPSi-CD and 33° for mPSi-CD) since the polymer layer presented very similar composition as previously shown by FTIR (Fig. 4).

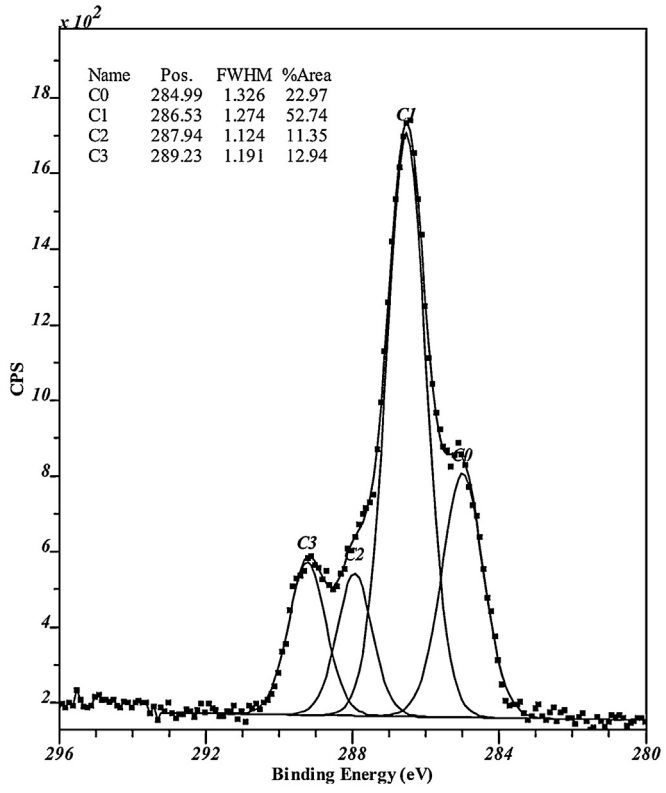

Fig. 6. C1s core level spectra of nPSi-CD.

The roughness and topography of the surface of samples were determined by means of AFM analyses. The obtained images are show in Fig. 8. The nPSi and nPSi-CO_x samples (Fig. 8a1 and a2) showed different root mean square roughness: 0.584 nm and 1.050 nm, respectively. This is reflected in the textured morphology of nPSi-CO_x surface, which is rounder than nPSi, which may be attributed to the post chemical treatment. In the case of mPSi and mPSi-CO_x (Fig. 8b1 and b2) both similar root mean square roughness values: 0.218 μm and 0.251 μm, respectively. Therefore, they did not show a significant morphologic change after chemical oxidation.

AFM images of samples functionalized with the βCD–CTR polymer are shown in Fig. 8a3 (nPSi-CD) and Fig. 8b3 (mPSi-CD). It is appreciable that the surfaces of both samples were covered by the polymer forming a different topography. They have similar root mean square roughness: 1.89 nm for nPSi-CD and 3.27 nm for mPSi-CD.

SEM analyses were performed to complete the study of the materials morphology at different stages of fabrication (Fig. 9). Morphological changes between non-oxidized samples and oxidized samples were not detected. The SEM images of oxidized samples, nPSi-CO_x and mPSi-CO_x, are show in Fig. 9a1 and b1, respectively. It can be observed that nPSi-CO_x layer has a thickness of 3.4 μm and an average pore diameter of 30 nm. In the case of mPSi-CO_x, the thickness is around 6.5 μm and the pore diameter is 0.6–1.2 μm. In both cases pores were columnar.

The SEM images of functionalized samples, nPSi-CD and mPSi-CD, are shown in Fig. 9a2 and b2, respectively. The synthesized polymer layer on the top surface of both samples had the same thickness (approximately 2.5 μm). Besides, it is appreciable that polymer infiltrates the porous matrix of both PSi substrates.

The binding between the PSi structures (nano- and macro-) and the βCD–CTR polymer can be understood in connection with previous characterization results. Firstly, as oxidized samples had a hydrophilic behavior, the aqueous monomer solution (Section 2.2) easily permeated into both porous substrates (nPSi-CO_x and mPSi-CO_x). Then, during *in-situ* polymerization, the βCD–CTR polymer was formed and chemisorbed onto the hydroxylated pore walls. Thus, the βCD–CTR polymer was well adhered to PSi pores by means of hydrogen bonding. Additionally, the porosity of samples worked as an anchor holding the polymer film (Figs. 8 and 9).

In order to measure the functionalization degree of polyCTR–βCD onto the nPSi and mPSi treated samples, it was necessary to retrieve the contribution of the silicon substrate to total weight (see Fig. 9). This was achieved by gravimetric and TGA measurements. The surface densities and calculated fixed polymer amounts are shown in Table 2. Results indicate a surfacic weight increase from oxidized samples to the functionalized ones from 0.49 to 1.16 mg/cm^2 (+136.74%) and from 1.79 to 2.64 mg/cm^2

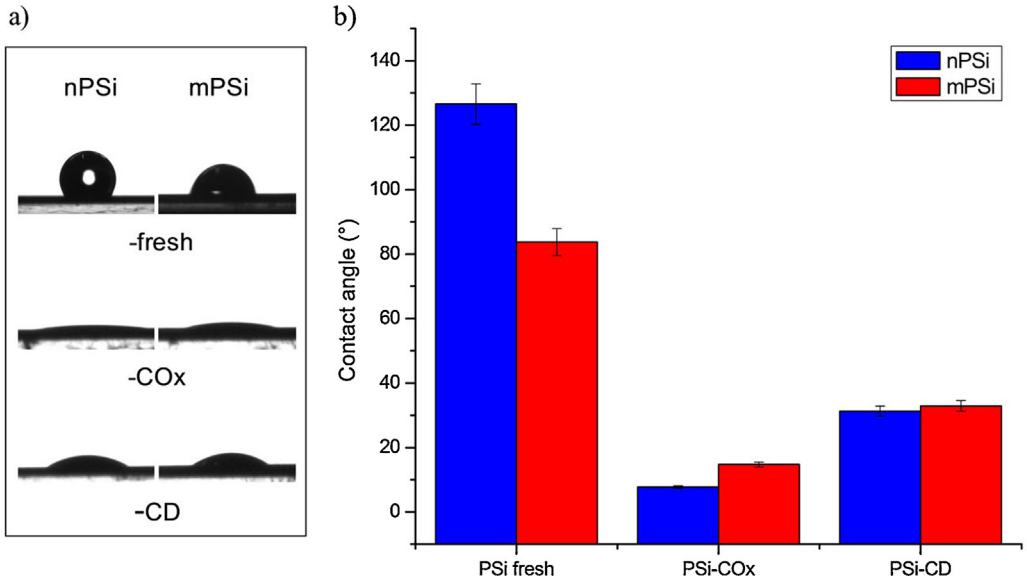

Fig. 7. Contact angle technique: (a) photographic sequence and b) plotted data.

Table 2
Surfacic mass and polymer amounts calculated from TGA.

Sample	mg PSi/cm^2	mg poly-CTR–βCD-PSi/cm^2	mg poly-CTR–βCD-/cm^2 PSi	mg poly-CTR–βCD-/mg PSi
nPSi-	0.49	1.16	0.67	1.37
mPSi-	1.79	2.64	0.85	0.47

(+47.79%) for nPSi and mPSi, respectively. The calculated amounts of polyCTR–βCD were 0.67 and 0.85 mg/cm^2, respectively. So, the polymer composition per surface area of PSi (mg/cm^2) was 1.27 times higher in mPSi-CD compared to nPSi-CD. Nevertheless, an inversion in the mass accumulated CD was observed by considering the weight of polyCTR–βCD per weight unit of nPSi and mPSi. The values were 1.37 and 0.47 mg/mg, respectively (right column of Table 2). In this latter case, the ponderal composition of nPSi-CD in polyCTR–βCD was 2.91 times that of mPSi-CD. This effect results from the large difference of surfacic mass between both PSi materials, as seen in the left column of Table 2.

The amount of immobilized polymer on PSi surfaces was also indirectly tested by detecting–COOH groups by TBO titration (Table 3). Nevertheless, data were reported as a function of area and mass of the bare PSi or composite, according to each case. For the composites (nPSi-CD and mPSi-CD), the polymer and PSi were considered as a whole. The loaded TBO by bare PSi substrates was scarcely detectable denoting the absence of –COOH groups, which correspond to previous chemical studies (ATR-FTIR and XPS). The TBO loaded per surface area in mPSi-CD (975 nmol/cm^2) was 110% higher than in nPSi-CD (463 nmol/cm^2) but the load per PSi mass unit was almost the same in both cases; just 8% more in nPSi-CD (400 nmol/mg) than mPSi-CD (370 nmol/mg).

Table 3
TBO titration.

Sample	nmol TBO/cm^2	nmol TBO/mg
nPSi-CO_x	39 (±4)	1 (±0.1)
nPSi-CD	463 (±4)	400 (±40)
mPSi-CO_x	8 (±0.8)	1 (±0.1)
mPSi-CD	975 (±90)	369 (±30)

3.2. Biological evaluation

As a preliminary biological evaluation, the cytocompatibility of the PSi-CD samples was tested *in-vitro* by studying the adhesion of L132 cells after 24 h of culture (Fig. 10). Cells adhered to the surfaces of all samples, giving a first positive estimation of biocompatibility (Blanchemain et al., 2008). However, the adherent cells on the samples also presented strong differences in morphology, indicating that the evolution of cells in terms of cell growth in longer culture experiment might be considerably different (Blanchemain et al., 2011). On nPSi, SEM images show that cells were isolated and presented a contracted semispherical form (Fig. 10a1) and few and short focal adhesions were identified (white arrows in Fig. 10a2). These two characteristics denote that cells did not fully-adhere on the substrate (Khung, Barritt, & Voelcker, 2008). In the case of cells on nPSi-CD, cells bodies were oval with extended lamellipodia (Fig. 10b1). Numerous focal adhesions extended around the body anchoring the cell to the surface (white arrows in Fig. 10b2). Those signs imply a better adhesion to the surface and their elongated cytoskeleton can be interpreted in terms of a migratory state (Khung et al., 2008). Cells on mPSi were spread and closely contacted to the surface (Fig. 10c1). Moreover, some focal adhesions are observed in the higher-magnification image in Fig. 10c2 (white arrows), which confirms that mPSi is better suited to support cells than nPSi (Sun, Puzas, Sheu, Liu, & Fauchet, 2007). Finally, it was found, in the case of mPSi-CD, that the polymer coating layer on the top surface was not strong enough to resist the cell culture or process of SEM sample preparation. The top polymer layer peeled off from the substrate (inset SEM image of Fig. 10d1) and probably carried away the adherent cells. Consequently, the cells were observed only in scattered areas of the sample. Relevantly, in spite of the absence of a top layer, there were pores refilled by polyCTR–βCD. The cell drastically elongated and slightly repelled substratum in their central area, minimizing contact with the surface (Fig. 10d1). Although there were no observable filopodia (Fig. 10d2), their long stretched shape further suggests a migratory state (Low et al., 2006). Despite their different cell growth behavior, cell cultures suggested the biocompatibility of the different composites tested, since epithelial cells can adopt an elongated or polarized form in culture when their protrusive lamellar activity is restricted to a limited region of the cell (Middleton, Brown, Brown, & Roberts, 1988).

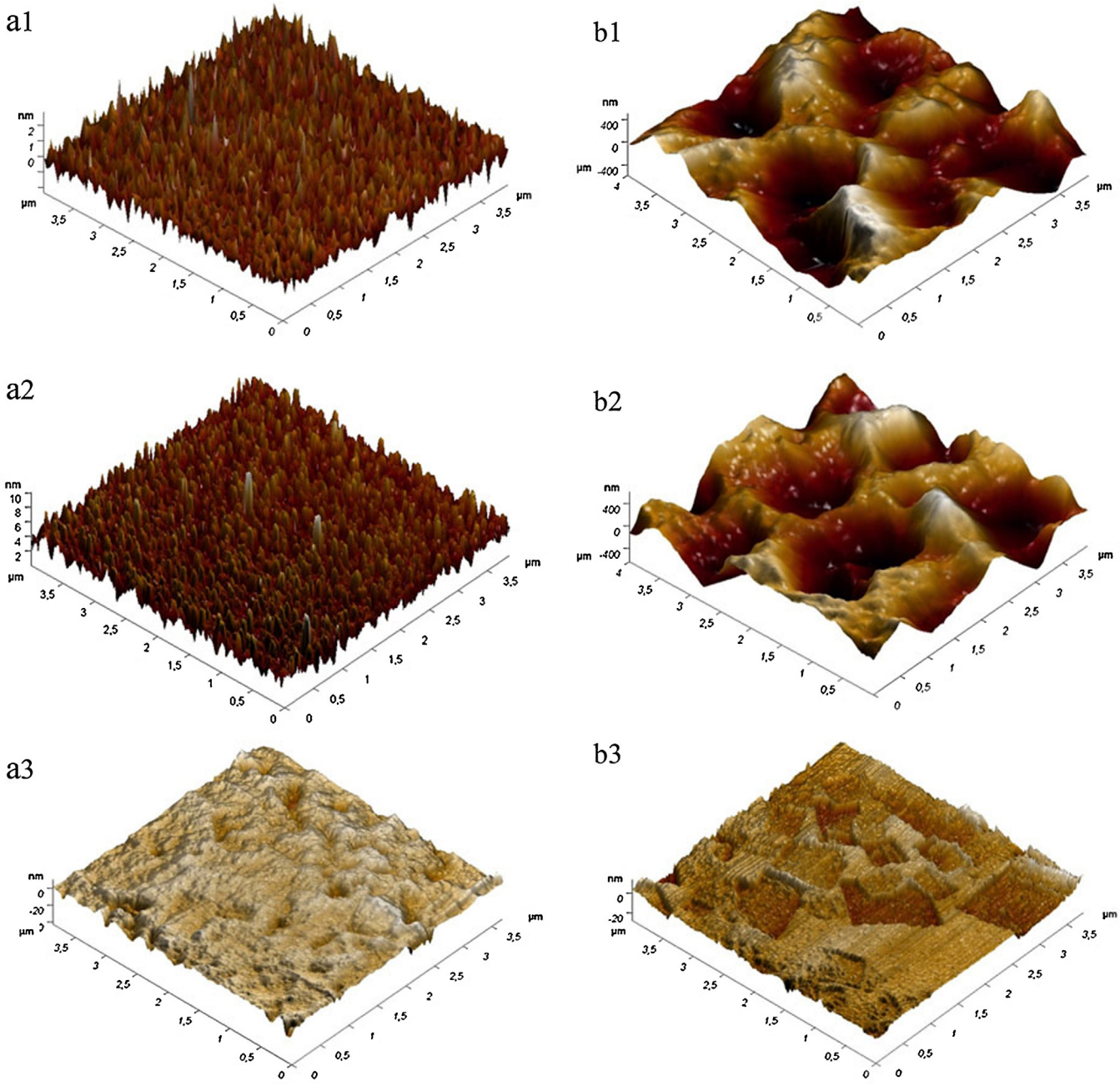

Fig. 8. 3D AFM images of (a1) nPSi, (b1) mPSi, (a2) nPSi-CO_x, (b2) mPSi-CO_x, (a3) nPSi-CD and (b3) mPSi-CD.

The restriction of lamellar activity in these cells may involve a different mechanism for each case, which can be tied to the surface chemistry of substrates (Low et al., 2006). Furthermore, physical characteristics of the substrate including nano- and microstructure play a crucial role in determining the behavior of cells in a given biological context (Reemann et al., 2013).

3.3. Drug delivery studies

In order to test the potential of the layered composite as a drug delivery system, samples were loaded with CFX and PDN. After drug loading, no morphological changes were observed by either SEM or AFM. However, changes in their chemical compositions were detected. The elemental surface compositions of the nPSi-CD before and after drug loadings was obtained from the XPS survey spectra and are presented in Table 4.

The loading of CFX is demonstrated by the appearance of N and the emerging of F signals (three and one atoms per CFX molecule, respectively, Fig. 3) and is not detected in the unloaded samples (Table 4). The analyses show also a slight surface contamination by silicon and, in the case of nPSi-CD-PDN, also nitrogen. The analysis of the C1s core level spectrum (Fig. 11b) further supports this conclusion. In fact, after CFX loading, the intensity of the hydrocarbon component at 285 eV increases slightly. Moreover, the FWHM of the C1 and C2 components increases, indicating the presence of C–N, CN(O) and C–F bonds (expected at about 287 eV). In addition, the C3 component shifts toward lower binding energy (about 0.22 eV) also supporting the formation of COO bonds. On the other hand, in the case of PDN loading, XPS analysis is not so indicative since there are no additional elements in PDN to those present on the nPSi-CD surface. However, the increase of the C3 (C=O) and C0 (C–C) components in the C1s core level spectra (Fig. 11c) are compatible with

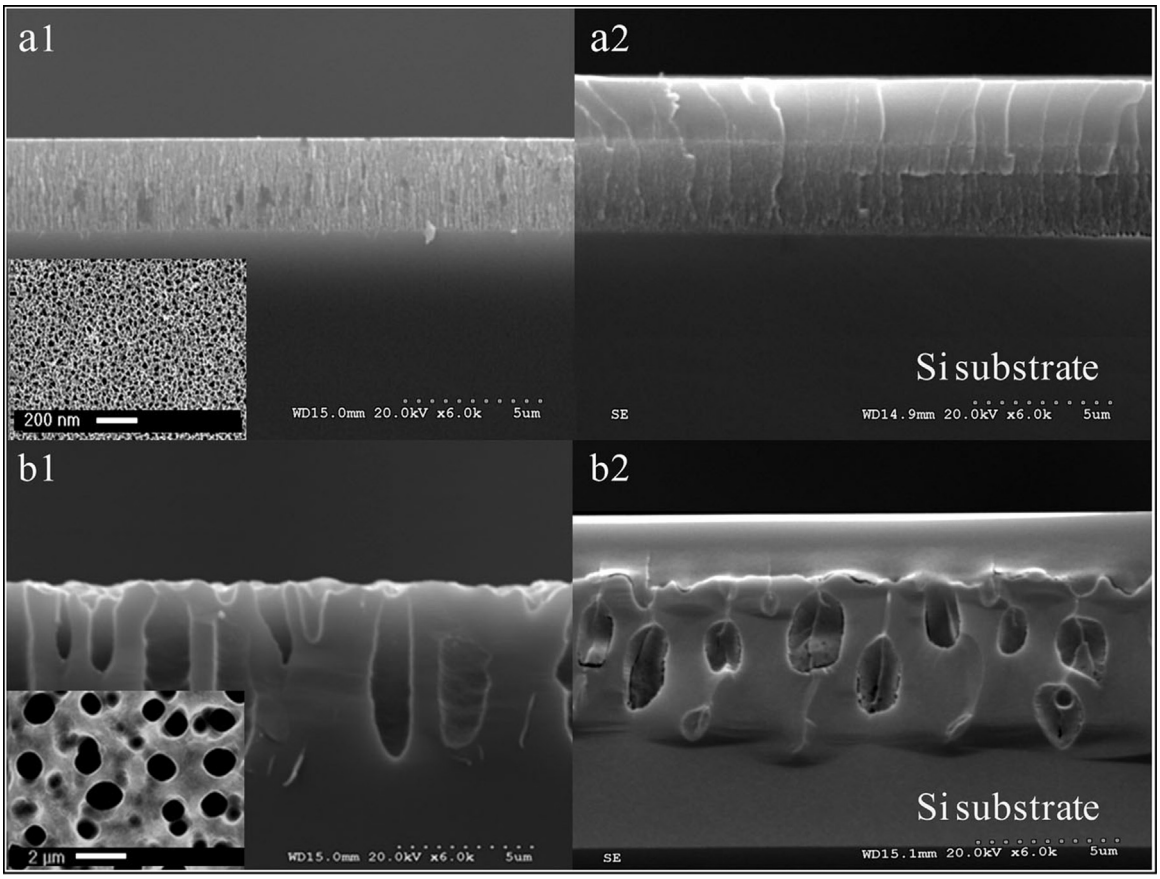

Fig. 9. SEM images of: (a1) cross-sectional and top view of nPSi-CO_x, (a2) cross-sectional view of nPSi-CD, (b1) cross-sectional and top view of mPSi-CO_x, and (b2) cross-sectional view of mPSi-CD.

an enrichment on PDN in view of the presence of two C=O carbons and 13 C–C carbons in the PDN molecule.

Although this analytical study refers to the surface of the samples, previous works have shown the formation of stable inclusion complexes between βCD and CFX (Blanchemain et al., 2012; Jianbin, Liang, Hao, & Dongpin, 2002) and PDN (Challa, Ahuja, Ali, & Khar, 2005; Larsen, Aachmann, Wimmer, Stella, & Kjolner, 2005), which suggests that these complexes may be also formed into the bulk of the PSi-CD matrix.

In a last step for evaluating the drug delivery functionality of the composites, the samples were tested with CFX and PDN in distilled water and PBS batches under stirring. The composites are stable in these media due to the neutral pH of the solutions, which remained at around 7 (Degoutin et al., 2012). High pH media were specifically avoided since PSi gets etched (Anderson, Elliott, Wallis, Canham, & Powell, 2003), and polyCTR–βCD becomes soluble through the hydrolysis of the ester linkages (Martel et al., 2005).

CFX release profiles are shown in Fig. 12. The profiles of Fig. 12a1 correspond to the drug release in function of sample area and the profiles of Fig. 12a2 report the drug release in function of sample mass, both in distilled water. The equivalent profiles obtained in PBS are shown in Fig. 12b1 and b2.

The four release profiles in Fig. 12 clearly show that CD functionalized PSi samples worked much better than CO_x control samples. The CO_x samples retained low amounts of drug, which were released during the first minutes. In the case of functionalized samples, the maximum yield of loaded drug per sample area was 140% higher in mPSi-CD than nPSi-CD. With regards to drug release as a function of sample mass, the increase was 19% higher in mPSi-CD than in nPSi-CD. These results matched with those obtained by TBO titrations. The time of CFX release was 40-fold faster in PBS medium (5 h) than distilled water (200 h). This could be originated by three main effects (Blanchemain et al., 2012): (a) The competitor role of ions in PBS towards drug-CD inclusion complex (the ions displace the drug from the CD ring). (b) The possible ionic interactions between the protonated amino functions of CFX and the carboxylate groups of polyCTR–βCD. In fact, these interactions may be screened by the exceeding counterions brought by PBS. (c) Because at neutral pH the carboxylic groups of CD's turn into carboxylate groups ionically repelling the CFX carboxylate group from the polymer network. A combination of these three aspects takes probably account for the accelerated release of CFX in PBS compared with a pure water medium.

The PDN release profiles are shown in Fig. 13 (in the same order as in Fig. 12). As in the previously described experiments, the CD

Table 4
Surface chemical compositions of nPSi-CD obtained before and after drug loadings from XPS analysis.

Sample	C (at%)	O (at%)	N (at%)	Si (at%)	F (at%)
nPSi-CD	56.9 (±0.5)	43.0 (±0.24)	–	–	–
nPSi-CD-CFX	61.5 (±0.3)	31.6 (±0.2)	4.5 (±0.24)	0.4 (±0.2)	1.4 (±0.2)
nPSi-CD-PDN	58.2 (±0.6)	40.4 (±0.53)	1.1 (±0.01)	0.1 (±0.02)	–

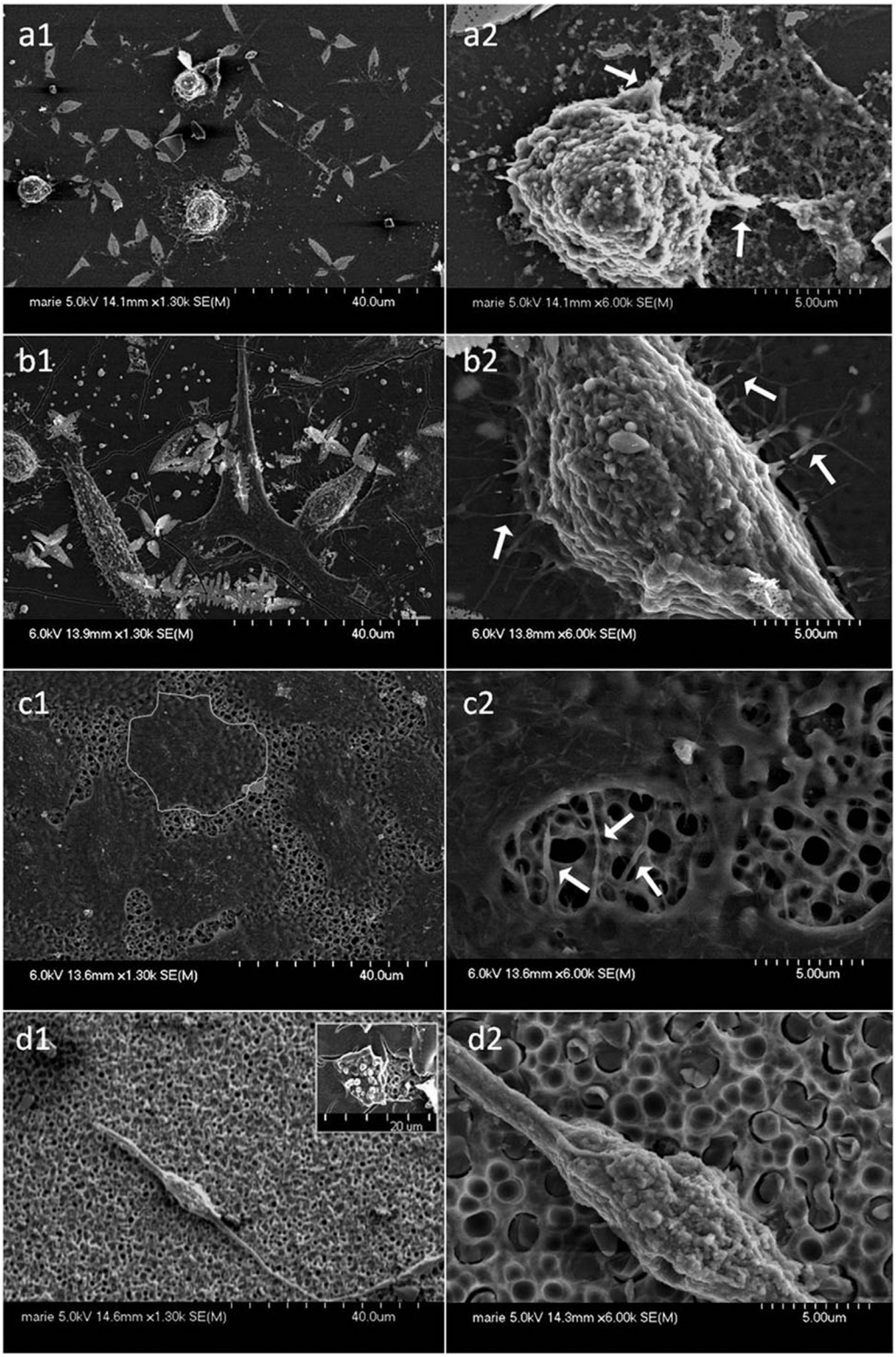

Fig. 10. SEM images after 24 h culture of L132 cells in: nPSi (a1 and a2), nPSi-CD (b1 and b2), mPSi (c1 and c2) and mPSi-CD (d1 and d2).

functionalized samples significantly retained more drug than the PSi ones when comparing as a function of surface area. However, when plotted as a function of sample mass, nPSi-CO_x releases more and faster than nPSi-CD. Nevertheless, the release of functionalized samples is more controlled than in the CO_x ones. The drug yield per sample area was 220% higher in mPSi-CD than in nPSi-CD, and per sample mass was 40% higher in mPSi-CD than in nPSi-CD. This tendency is also similar to what was observed for CFX and during TBO titration. Functionalization degrees per sample area magnify delivery rates in favor of mPSi-CD, although data expressed as a function of mass do not show such significant differences. The release time was also affected by the medium of release. The PDN release was around 30-fold faster in PBS medium (2.5 h) than in distilled water (75 h).

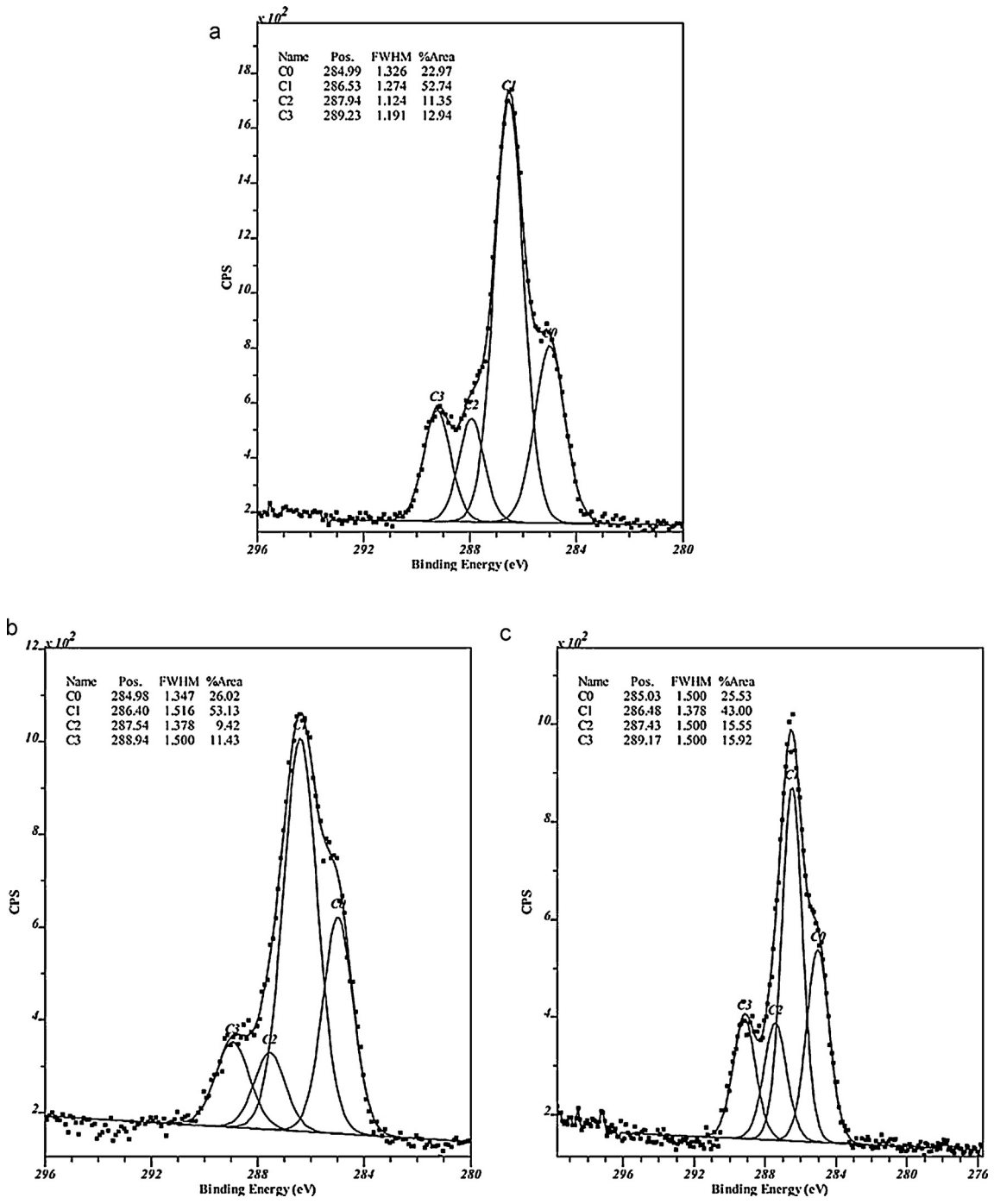

Fig. 11. C1s core level spectra of (a) nPSi-CD, (b) after CFX loading and c) after PDN loading.

Table 5
In-vitro release kinetics of CFX and PND in distilled water and PBS.

Sample	Drug	Medium	Korsmeyer–Peppas model			Kinetics mechanisms
			n	*k*	r^2	
nPSi-CD	CFX	Distilled water	0.2770	0.1824	0.9382	Fickian diffusion
		PBS	0.5464	0.8933	0.9905	Fickian diffusion
	PDN	Distilled water	0.3789	0.2780	0.9325	Fickian diffusion
		PBS	0.3564	0.7782	0.9976	Fickian diffusion
mPSi-CD	CFX	Distilled water	0.5251	0.0516	0.9788	Fickian diffusion
		PBS	0.8505	0.8828	0.9835	Non-Fickian
	PDN	Distilled water	0.2386	0.5544	0.9989	Fickian diffusion
		PBS	0.2777	0.8443	0.9843	Fickian diffusion

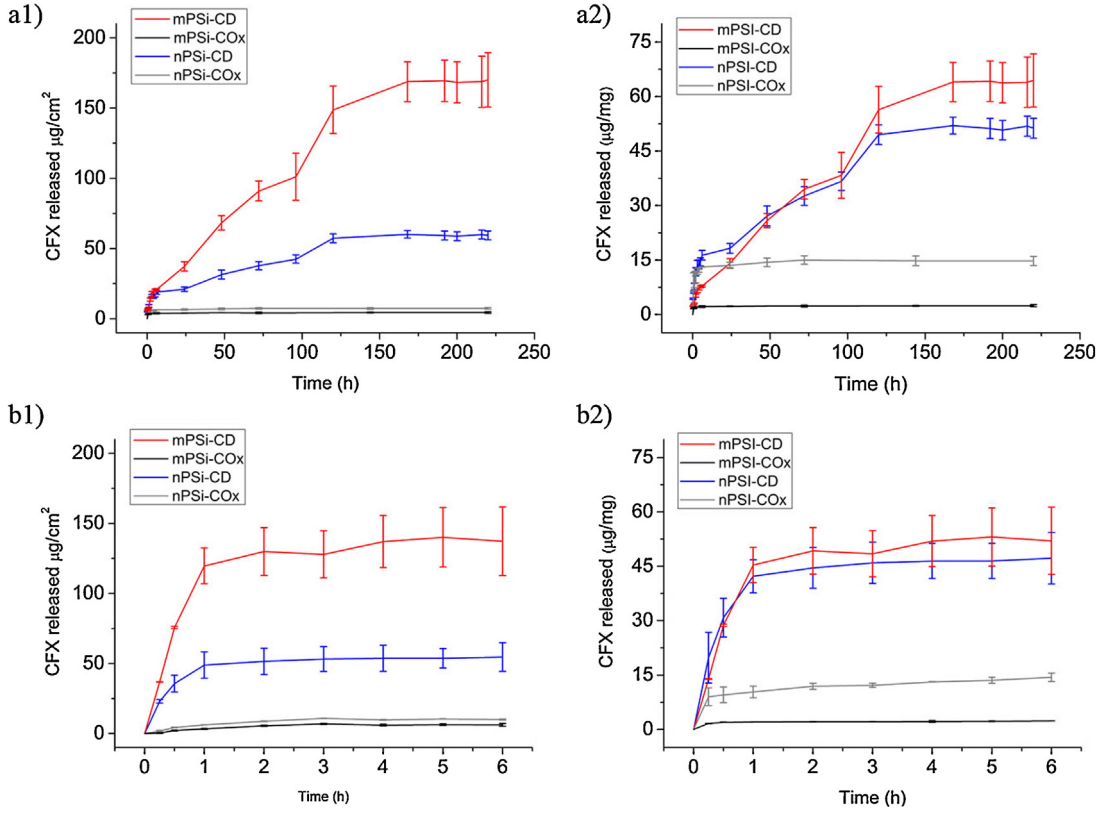

Fig. 12. CFX release profiles in distilled water per sample area (a1) and per sample mass (a2), and in PBS per sample area (b1) and per sample mass (b2).

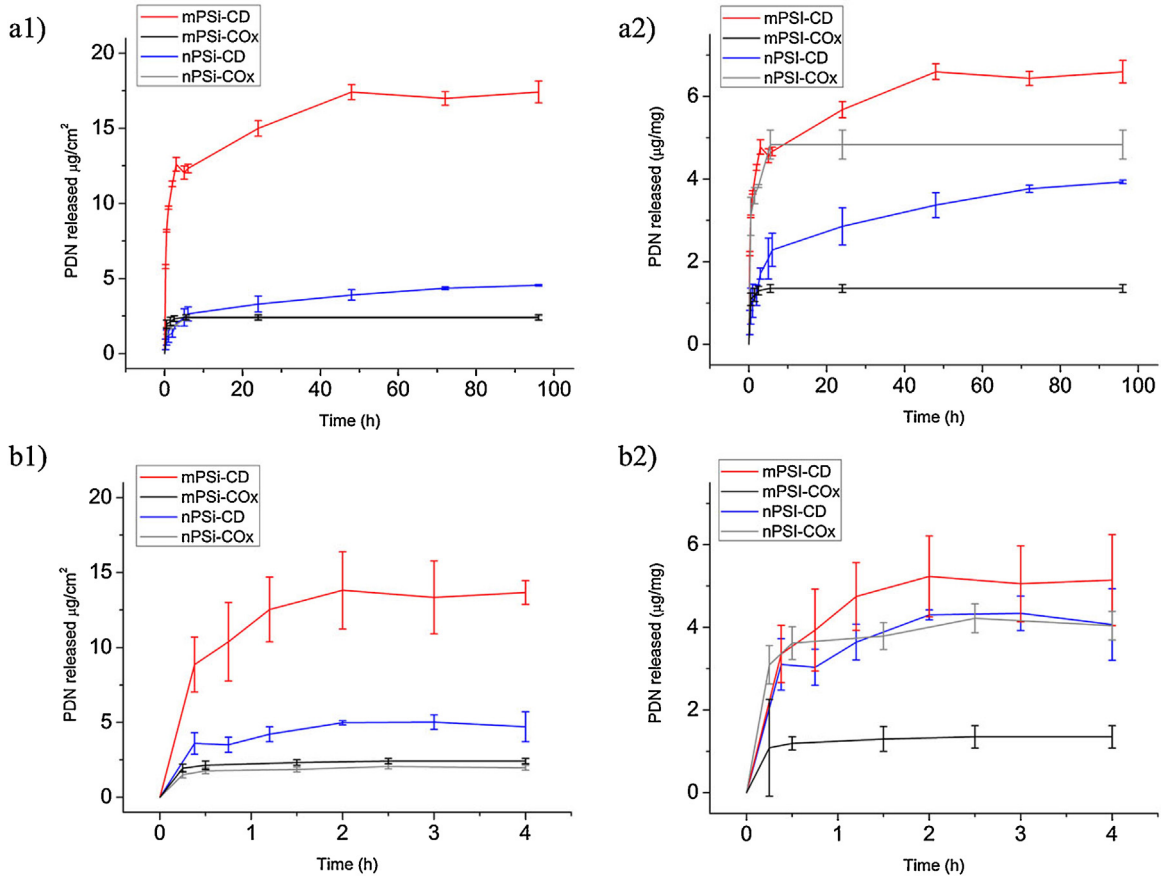

Fig. 13. PDN release profiles in distilled water per sample area (a1) and per sample mass (a2), and in PBS per sample area (b1) and per sample mass (b2).

From Figs. 12 and 13, it is possible to state that CFX is more compatible with both composites (nPSi-CD and mPSi-CD) than PDN. CFX load was 10-fold more that corresponding to PDN. On the other hand, the release time was also longer for CFX than for PDN in both composites: 2.7 times longer in distilled water and 2 times longer in PBS. The higher affinity of composites for CFX than PDN can be explained by the presence of an aromatic fluor, a piperazinyl, and a cyclopropane substituent in CFX. Thus, CFX can interact with the polyCTR–βCD not only by host–guest interactions, but also by ionic exchange with the carboxylic groups of the polymer according to: substrate-COOH/CFX-piperaz → substrate-COO^-/CFX-piperaz-H^+. In a previous paper, we disclosed that CFX was adsorbed in majority through ionic interactions with the polyCTR–βCD, compared to host–guest complexation (Blanchemain et al., 2012).

Concerning the inclusion complex formation constant: (3479 and 270 M^{-1} for PDN and CFX, respectively (Jianbin et al., 2002; Larsen et al., 2005)), both values clearly indicate that most of the CD cavities on the polyCTR–βCD are occupied by both guests at equilibrium, but it cannot be stated that cavity occupation rates for both drugs is proportional to the given constants. To conclude, in the case of CFX, sorption by the polyCTR–βCD is mainly driven by ionic interactions, on the contrary for PDN, mainly host–guest complexation occurs. This explains why CFX adsorption/desorption is ten fold that corresponding to PDN.

In order to glean deeper insight into the mechanisms that govern the release of CFX and PDN in distilled water and PBS from both composites, the Korsmeyer–Peppas semi-empirical model was fitted to the release data. This study was not applied to bare PSi substrates due to their fast and uncontrolled drug release in most cases. Their data were not available to manipulate mathematically according to the restriction of the model (M_t/M_∞ data in the 0.1–0.6 range).

When the Korsmeyer–Peppas is applied to thin films (Lucht & Peppas, 1987; Lin & Metters, 2006; Costa, 2001) the release exponent $n = 0.5$, or $n \leq 0.5$ (Glisoni et al., 2013; Chime Salome, Onunkwo Godswill, & Onyishi Ikechukwu, 2013; Souza, Ardisson, & Sousa, 2009), corresponds to a Fickian diffusion release during which the solvent penetration is the rate limiting step; $0.5 < n < 1.0$ is related to non-Fickian release, this means that drug release followed both diffusion and erosion controlled mechanisms, and $n = 1$ corresponds to zero order release, where drug release is independent of time. Table 5 shows the results achieved applying the Korsmeyer–Peppas model to composites. According to the release exponent n obtained in most cases (0.5 or lower), the drug release kinetics of the systems were governed by a Fickian process. However, there was an important difference between the k values when they are compared as a function of the medium. The drug profiles in PBS showed significantly higher k values than in distilled water, which is coherent with a faster release. Besides, as k is related to drug/polymer interaction, these results would confirm the competitor role of ions in PBS towards drug-CD inclusion complex, previously exposed.

This work is mainly focused on synthesis and physicochemical characterization issues. Although a preliminary cytocompatibility test was carried out in the obtained composites, further biological characterizations should be performed in order to assure their use for *in-vivo* applications, such as MTT and CCK-O8 assays. However, as composites were tested with two drugs that could be used in post-ophthalmic surgery (Oliver et al., 2005; Ravindran et al., 2009), their use as intraocular drug delivery system could be pre-evaluated as a function of the required drug concentration for medical therapy. Besides, PSi-based composites have recently been already used successfully in ophthalmic surgery (Muñoz Noval et al., 2012).

It is reported that the minimum inhibitory concentration of CFX required to inhibit the growth of 90% of microorganisms (MIC90) goes from less than 0.25–2 μg/mL (Yu-Speight, Kern, & Erb, 2005) (less than 0.25 μg/ml for *Bacillus* sp. and *Escherchia coli*, while 0.5 μg/mL for *Corynebacterium* sp. and *Staphylococcus* sp., and 2 μg/mL for *Streptococcus* sp.). As the mean volume of an adult human eye is 6.5 mL (Festa et al., 2012), the required amount of CFX into the eye for a medical therapy is around 13 μg, a value not only reached but exceeded with just 1 mg of both PSi-CD composites synthesized. In the case of the use of PDN as an ocular anti-inflammatory, a minimum concentration of 25 ng/mL is necessary to suppress inflammation and minimize side effects of ophthalmic steroids such as bulbar perforation, choroidal injection, central retinal artery occlusion and others (McGhee, 1992). We can thus estimate that 0.16 μg of PDN are required for a medical therapy. This value is also reached by both PSi-CD composites in the kinetic studies. On the other hand, due to the thin layered morphology of composites, they could be intravitreally injected (Muñoz Noval et al., 2012) during any eye surgery in order to reduce inflammation of the eye derived from an infectious agent after the surgery (Olson, 2004).

4. Conclusions

Results from FTIR, XPS and water contact angle indicated that nanoporous and macroporous PSi layers were properly stabilized by chemical oxidation and further functionalized by βCD *in-situ* polymerization using CTR as a crosslinking agent. Microscopic characterization showed clear topographic changes of the surfaces after each step (AFM) and that a polymer is integrated in PSi pores and top surface (SEM). The amalgamation between the porous matrix of samples and polymer was generated by two main phenomena: the PSi hydrophilic compatibility with the external wall of CD after chemical oxidation, and the anchoring effect of the porous matrix. On the other hand, as a preliminary biological evaluation, the deposition and *in-vitro* proliferation of L132 cells on both reference samples and both composites suggested their cytocompatibility, despite their different cell growth behaviors on each sample.

The drug release profiles show that functionalized samples released drugs for longer time than CO_x ones. Higher drug loads are also achieved and provide a better-controlled release. The profiles were reported in two ways, normalized to area and normalized to mass of sample. The results significantly favor mPSi-CD with respect to nPSi-CD when normalized to area, but when results are normalized to mass they are similar.

The studies also indicate that CFX is more compatible with both composites (nPSi-CD and mPSi-CD) than PDN: CFX load was 10 times higher than PDN load in both composites. On the other hand, the release time for CFX was longer than for PDN in both composites: one week in distilled water and 5 h in PBS for CFX; three days in distilled water and 2.5 h in PBS for PDN. The faster release in PBS is due to the ionic strength of salts in solution. According to the Korsmeyer–Peppas semi-empirical model, the drug release kinetics was governed by a Fickian process.

In summary, characterization techniques and *in-vitro* drug release studies showed the potential of layered composites of PSi and β-CD–CTR polymer as functional devices for drug delivery applications.

Acknowledgments

This project was financed by Madrid Regional Grant "Microseres" and project "Producción de patrones con haces iónicos en materiales para aplicaciones biomédicas y fotónicas MAT2011-28345-C02-01" from the ministry of economy and competitivity. J. Hernandez-Montelongo thanks the European Commission for his research grant from the program "Erasmus Mundus External Cooperation Windows Lot 20".

References

Anderson, S. H. C., Elliott, H., Wallis, D. J., Canham, L. T., & Powell, J. J. (2003). Dissolution of different forms of partially porous silicon wafers under simulated physiological conditions. *Physica Status Solidi (a)*, *197*(2), 331–335.

Anglin, E. J., Cheng, L., Freeman, W. R., & Sailor, M. J. (2008). Porous silicon in drug delivery devices and materials. *Advanced Drug Delivery Reviews*, *60*(11), 1266–1277.

Bemason, G. D. B. (1992). *The XPS of polymer database*. UK: Surface Spectra.

Bisi, O., Ossicini, S., & Pavesi, L. (2000). Porous silicon: A quantum sponge structure for silicon based optoelectronics. *Surface Science Reports*, *38*(1), 1–126.

Blanchemain, N., Aguilar, M., Chai, F., Jimenez, M., Jean-Baptiste, E., El-Achari, A., et al. (2011). Selective biological response of human pulmonary microvascular endothelial cells and human pulmonary artery smooth muscle cells on cold-plasma-modified polyester vascular prostheses. *Biomedical Materials*, *6*(6), 065003.

Blanchemain, N., Chai, F., Haulon, S., Krump-Konvalinkova, V., Traisnel, M., Morcellet, M., et al. (2008). Biological behaviour of an endothelial cell line (HPMEC) on vascular prostheses grafted with hydroxypropylgamma-cyclodextrine (HPγ-CD) and hydroxypropylbeta-cyclodextrine (HPβ-CD). *Journal of Materials Science Materials in Medicine*, *19*(6), 2515–2523.

Blanchemain, N., Karrout, Y., Tabary, N., Bria, M., Neut, C., Hildebrand, H., et al. (2012). Comparative study of vascular prostheses coated with polycyclodextrins for controlled ciprofloxacin release. *Carbohydrate Polymers*, *90*, 1695–1703.

Challa, R., Ahuja, A., Ali, J., & Khar, R. (2005). Cyclodextrins in drug delivery: An updated review. *AAPS PharmSciTech*, *6*(2), E329–E357.

Chime Salome, A., Onunkwo Godswill, C., & Onyishi Ikechukwu, I. (2013). Kinetics and mechanisms of drug release from swellable and non swellable matrices: A review. *Research Journal of Pharmaceutical, Biological and Chemical Sciences*, *4*(2), 97–103.

Coffer, J. L., Whitehead, M. A., Nagesha, D. K., Mukherjee, P., Akkaraju, G., Totolici, M., et al. (2005). Porous silicon-based scaffolds for tissue engineering and other biomedical applications. *Physica Status Solidi (a)*, *202*(8), 1451–1455.

Costa, P., & Sousa Lobo, J. M. (2001). Modeling and comparison of dissolution profiles. *European Journal of Pharmaceutical Sciences: Official Journal of the European Federation for Pharmaceutical Sciences*, *13*(2), 123–133.

Davis, M. E. (2009). Design and development of IT-101, a cyclodextrin-containing polymer conjugate of camptothecin. *Advanced Drug Delivery Reviews*, *61*(13), 1189–1192.

Davis, M. E., & Brewster, M. E. (2004). Cyclodextrin-based pharmaceutics: Past, present and future. *Nature Reviews. Drug Discovery*, *3*(12), 1023–1035.

Degoutin, S., Jimenez, M., Casetta, M., Bellayer, S., Chai, F., Blanchemain, N., et al. (2012). Anticoagulant and antimicrobial finishing of non-woven polypropylene textiles. *Biomedical Materials*, *7*(3), 035001.

Dhanekar, S., & Jain, S. (2013a). Porous silicon biosensor: Current status. *Biosensors and Bioelectronics*, *41*, 54–64.

Dhanekar, S., & Jain, S. (2013b). Porous silicon biosensor: Current status. *Biosensors & Bioelectronics*, *41*, 54–64.

El Ghoul, Y., Blanchemain, N., Laurent, T., Campagne, C., El Achari, A., Roudesli, S., et al. (2008). Chemical, biological and microbiological evaluation of cyclodextrin finished polyamide inguinal meshes. *Acta Biomaterialia*, *4*(5), 1392–1400.

Festa, F., Pagnoni, M., Valerio, R., Rodolfino, D., Saccucci, M., d'Attilio, M., et al. (2012). Orbital volume and surface after Le Fort III advancement in syndromic craniosynostosis. *Journal of Craniofacial Surgery*, *23*(3), 789–792.

Föll, H., Christophersen, M., Carstensen, J., & Hasse, G. (2002). Formation and application of porous silicon. *Materials Science and Engineering Reports*, *39*(4), 93–141.

Glisoni, R. J., García-Fernández, M. J., Pino, M., Gutkind, G., Moglioni, A. G., Alvarez-Lorenzo, C., et al. (2013). β-Cyclodextrin hydrogels for the ocular release of antibacterial thiosemicarbazones. *Carbohydrate Polymers*, *93*, 449–4457.

Gorbanyuk, T., Evtukh, A., Litovchenko, V., Solnsev, V., & Pakhlov, E. (2006). Porous silicon microstructure and composition characterization depending on the formation conditions. *Thin Solid Films*, *495*(1), 134–138.

Hernández-Montelongo, J., Muñoz-Noval, A., Torres-Costa, V., Martín-Palma, R., & Manso-Silvan, M. (2012). Cyclic calcium phosphate electrodeposition on porous silicon. *International Journal of Electrochemical Science*, *7*, 1840–1851.

Izawa, H., Kawakami, K., Sumita, M., Tateyama, Y., Hill, J. P., & Ariga, K. (2013). β-Cyclodextrin-crosslinked alginate gel for patient-controlled drug delivery systems: Regulation of host–guest interactions with mechanical stimuli. *Journal of Materials Chemistry B*, *1*(16), 2155–2161.

Jianbin, C., Liang, C., Hao, X., & Dongpin, M. (2002). Preparation and study on the solid inclusion complex of ciprofloxacin with b-cyclodextrin. *Spectrochimica Acta, Part A: Molecular and Biomolecular Spectroscopy*, *58*, 2809–2815.

Khung, Y., Barritt, G., & Voelcker, N. (2008). Using continuous porous silicon gradients to study the influence of surface topography on the behaviour of neuroblastoma cells. *Experimental Cell Research*, *314*(4), 789–800.

Korsmeyer, R. W., Gurny, R., Doelker, E., Buri, P., & Peppas, N. A. (1983). Mechanisms of solute release from porous hydrophilic polymers. *International Journal of Pharmaceutics*, *15*(1), 25–35.

Lane, S. S., & Holland, E. J. (2012). Loteprednol etabonate 0.5% versus prednisolone acetate 1.0% for the treatment of inflammation after cataract surgery. *Journal of Cataract and Refractive Surgery*, *39*(2), 168–173.

Larsen, K., Aachmann, F., Wimmer, R., Stella, V., & Kjolner, U. (2005). Phase solubility and structure of the inclusion complexes of prednisolone and 6a-methyl prednisolone with various cyclodextrins. *Journal of Pharmaceutical Sciences*, *94*(3), 507–515.

Leprêtre, S., Chai, F., Hornez, J. C., Vermet, G., Neut, C., Descamps, M., et al. (2009). Prolonged local antibiotics delivery from hydroxyapatite functionalised with cyclodextrin polymers. *Biomaterials*, *30*(30), 6086–6093.

Li, J., Ni, X., & Leong, K. W. (2003). Injectable drug-delivery systems based on supramolecular hydrogels formed by poly (ethylene oxide) s and α-cyclodextrin. *Journal of Biomedical Materials Research Part A*, *65*(2), 196–202.

Lin, C., & Metters, A. T. (2006). Hydrogels in controlled release formulations: Network design and mathematical modeling. *Advanced Drug Delivery Reviews*, *58*(12), 1379–1408.

Liu, G., Jin, Q., Liu, X., Lv, L., Chen, C., & Ji, J. (2011). Biocompatible vesicles based on PEO-b-PMPC/α-cyclodextrin inclusion complexes for drug delivery. *Soft Matter*, *7*(2), 662–669.

Low, S. P., Williams, K. A., Canham, L. T., & Voelcker, N. H. (2006). Evaluation of mammalian cell adhesion on surface-modified porous silicon. *Biomaterials*, *27*(26), 4538–4546.

Lucht, L. M., & Peppas, N. A. (1987). Transport of penetrants in the macromolecular structure of coals. V. Anomalous transport in pretreated coal particles. *Journal of Applied Polymer Science*, *33*(5), 1557–1566.

Martel, B., Ruffin, D., Weltrowski, M., Lekchiri, Y., & Morcellet, M. (2005). Water-soluble polymers and gels from the polycondensation between cyclodextrins and poly(carboxylic acid)s: A study of the preparation parameters. *Journal of Applied Polymer Science*, *97*(2), 433–442.

Martin, A., Tabary, N., Leclercq, L., Junthip, J., Degoutin, S., Aubert-Viard, F., et al. (2013). Multilayered textile coating based on a β-cyclodextrin polyelectrolyte for the controlled release of drugs. *Carbohydrate Polymers*, *93*, 718–730.

Martin-Palma, R. J., Manso-Silvan, M., & Torres-Costa, V. (2010). Biomedical applications of nanostructured porous silicon: A review. *Journal of Nanophotonics*, *4*(042502), 1–20.

Mawhinney, D. B., Glass, J. A., Jr., & Yates, J. T., Jr. (1997). FTIR study of the oxidation of porous silicon. *Journal of Physical Chemistry B*, *101*(7), 1202–1206.

McGhee, C. (1992). Pharmacokinetics of ophthalmic corticosteroids. *British Journal of Ophthalmology*, *76*(11), 681–684.

Middleton, C., Brown, A., Brown, R., & Roberts, D. (1988). The shape of cultured epithelial cells does not depend on the integrity of their microtubules. *Journal of Cell Science*, *91*(3), 337–345.

Mukherjee, P., Whitehead, M. A., Senter, R. A., Fan, D., Coffer, J. L., & Canham, L. T. (2006). Biorelevant mesoporous silicon/polymer composites: Directed assembly, disassembly, and controlled release. *Biomedical Microdevices*, *8*(1), 9–15.

Muñoz Noval, A., García, R., Ruiz Casas, D., Losada Bayo, D., Sánchez Vaquero, V., Costa, V. T., et al. (2012). Design and characterization of biofunctional magnetic porous silicon flakes. *Acta Biomaterialia*, *9*, 6169–6176.

Naveas, N., Costa, V. T., Gallach, D., Hernandez-Montelongo, J., Palma, R. J. M., Garcia-Ruiz, J. P., et al. (2012). Chemical stabilization of porous silicon for enhanced biofunctionalization with immunoglobulin. *Science and Technology of Advanced Materials*, *13*(4), 045009.

Noval, A. M., Vaquero, V. S., Quijorna, E. P., Costa, V. T., Pérez, D. G., Méndez, L. G., et al. (2012). Aging of porous silicon in physiological conditions: Cell adhesion modes on scaled 1D micropatterns. *Journal of Biomedial Materials Research A*, *100*(6), 1615–1622.

Ogata, Y., Niki, H., Sakka, T., & Iwasaki, M. (1995). Oxidation of porous silicon under water vapor environment. *Journal of the Electrochemical Society*, *142*(5), 1595–1601.

Oliver, K. M., Strube, Y. N. J., Mohan, S. K., & Slomovic, A. R. (2005). Fourth-generation fluoroquinolones in the treatment of mycobacterial infectious keratitis after laser-assisted in situ keratomileusis surgery. *Canadian Journal of Ophthalmology. Journal Canadien d'Ophtalmologie*, *40*(6), 750–753.

Olson, R. J. (2004). Reducing the risk of postoperative endophthalmitis. *Survey of Ophthalmology*, *49*(2), S55–S61.

Ravindran, R. D., Venkatesh, R., Chang, D. F., Sengupta, S., Gyatsho, J., & Talwar, B. (2009). Incidence of post-cataract endophthalmitis at Aravind Eye Hospital. *Journal of Cataract and Refractive Surgery*, *35*(4), 629–636.

Reemann, P., Kangur, T., Pook, M., Paalo, M., Nurmis, L., Kink, I., et al. (2013). Fibroblast growth on micro-and nanopatterned surfaces prepared by a novel sol–gel phase separation method. *Journal of Materials Science Materials in Medicine*, *24*, 783–792.

Seah, M., Spencer, S., Bensebaa, F., Vickridge, I., Danzebrink, H., Krumrey, M., et al. (2004). Critical review of the current status of thickness measurements for ultrathin SiO_2 on Si Part V: Results of a CCQM pilot study. *Surface and Interface Analysis*, *36*(9), 1269–1303.

Segal, E., Perelman, L. A., Cunin, F., Di Renzo, F., Devoisselle, J. M., Li, Y. Y., et al. (2007). Confinement of thermoresponsive hydrogels in nanostructured porous silicon dioxide templates. *Advanced Functional Materials*, *17*(7), 1153–1162.

Souza, K., Ardisson, J., & Sousa, E. (2009). Study of mesoporous silica/magnetite systems in drug controlled release. *Journal of Materials Science Materials in Medicine*, *20*(2), 507–512.

Stewart, M. P., & Buriak, J. (2000). Chemical and biological applications of porous silicon technology. *Advanced Materials*, *12*(12), 859–869.

Struck, H., & Bariszlovich, A. (2001). Comparison of 0.1% dexamethasone phosphate eye gel (Dexagel) and 1% prednisolone acetate eye suspension in the treatment of post-operative inflammation after cataract surgery. *Graefe's Archive for Clinical and Experimental Ophthalmology = Albrecht von Graefes Archiv fur klinische und experimentelle Ophthalmologie*, *239*(10), 737–742.

Sun, W., Puzas, J. E., Sheu, T., Liu, X., & Fauchet, P. M. (2007). Nano-to microscale porous silicon as a cell interface for bone-tissue engineering. *Advanced Materials*, *19*(7), 921–924.

Taha, M., Chai, F., Blanchemain, N., Goube, M., Martel, B., & Hildebrand, H. (2013). Validating the poly-cyclodextrins based local drug delivery system on plasma-sprayed hydroxyapatite coated orthopedic implant with toluidine blue O. *Materials Science and Engineering C*, *33*, 2639–2647.

Tanaka, T., Mangala, L. S., Vivas-Mejia, P. E., Nieves-Alicea, R., Mann, A. P., Mora, E., et al. (2010). Sustained small interfering RNA delivery by mesoporous silicon particles. *Cancer Research*, *70*(9), 3687–3696.

Thrimawithana, T. R., Young, S., Bunt, C. R., Green, C., & Alany, R. G. (2011). Drug delivery to the posterior segment of the eye. *Drug Discovery Today*, *16*(5), 270–277.

Tolstoy, V. P., Chernyshova, I., & Skryshevsky, V. A. (2003). *Handbook of infrared spectroscopy of ultrathin films*. USA: Wiley-VCH.

Trotta, F., Zanetti, M., & Cavalli, R. (2012). Cyclodextrin-based nanosponges as drug carriers. *Beilstein Journal of Organic Chemistry*, *8*(1), 2091–2099.

Ulgut, B., & Suzer, S. (2003). XPS studies of SiO_2/Si system under external bias. *Journal of Physical Chemistry B*, *107*(13), 2939–2943.

Yu-Speight, A. W., Kern, T. J., & Erb, H. N. (2005). Ciprofloxacin and ofloxacin aqueous humor concentrations after topical administration in dogs undergoing cataract surgery. *Veterinary Ophthalmology*, *8*(3), 181–187.

Zhao, D., Zhao, L., Zhu, C., Tian, Z., & Shen, X. (2009). Synthesis and properties of water-insoluble β-cyclodextrin polymer crosslinked by citric acid with PEG-400 as modifier. *Carbohydrate Polymers*, *78*(1), 125–130.